# A Compact Underwater WPT System With Load-Independent Current Output Characteristic Under Wide Range of Coupling Coefficient

Jiayuan Li, Kehan Zhang, *Member, IEEE*, Zhengchao Yan, *Member, IEEE*, Haibing Wen, Baidong Peng, and Jipan Wang

***Abstract*—Wireless power transfer (WPT) technology provides an effective solution to the power supply of autonomous underwater vehicle (AUV). However, the misalignments and rotation often occur between the docking station and AUV, which would result in a fluctuation to system's output characteristics. To maintain constant current output with unreliable communication under seawater environment is a barrier. Aiming at this problem, this article presented an *LCC*-N WPT system with fewer compensation devices on the receiver side, which is immensely suitable for reducing the weight and volume of the AUV. Meanwhile, based on the switch-controlled capacitance (SCC) technology and frequency modulation at the transmitter side, the mentioned WPT system could stabilize the output current while the coupling coefficient $k$ and load resistance $R_L$ undergo a wide range variation. The determination method of system parameters, including operation frequency, capacitance value of SCC and compensation inductance under various misalignment conditions was detailed derived. Besides, the zero phase angle characteristic could be achieved during the whole process. The experimental results indicate that while the coupling coefficient varies from 0.3 to 0.54, the fluctuation of output current for the proposed WPT system is less than 4.47% and the power transfer efficiency could be maintained above 87%, and the maximum efficiency can reach 92.8%. In addition, the characteristics of load-independent output current during the misalignment process was also verified.**

***Index Terms*—Constant current, misalignment tolerance, switch-controlled capacitance (SCC), underwater wireless power transfer (WPT).**

## I. Introduction

WIRELESS power transfer (WPT) technology for autonomous underwater vehicle (AUV) has demonstrated outstanding performance in improving the safety and invisibility of underwater power supply [1], [2], [3], [4]. While the AUV is about to run out of power, it could be recharged by docking in the nearby underwater wireless charging platform. However, in the actual operation of the above process, owing to the influence of navigation guidance technology and intricate marine environments, the docking accuracy between AUVs and underwater charging stations is difficult to obtain assurance, which will directly lead to radial, axial misalignments and rotation between the transmitter coil and receiver coil, as shown in Fig. 1. The magnetic coupler misalignment will further cause the coupling coefficient $k$ undergoes a wide range of variation, which would give rise to dramatic fluctuation of the output characteristic in the WPT system. For presenting to smoothly and accurately dock the AUV with charging station, Wu et al. [5] proposed a funnel-type docking station design based on acoustic and optical combination guiding method and a position locking mechanism, but the additional navigation guidance devices and locking mechanisms greatly increase the cost and weight of the system. In [6], a magnetic coupler with variable ring-shaped was designed to eliminate the gap between the AUV and charging station. Nonetheless, the complex mechanical structure reduces the reliability of the system in underwater environment.

Currently, many studies are focused on improving misalignment tolerance for the AUV WPT system by ingenious magnetic coupler design [7], [8]. The key ideology of this method

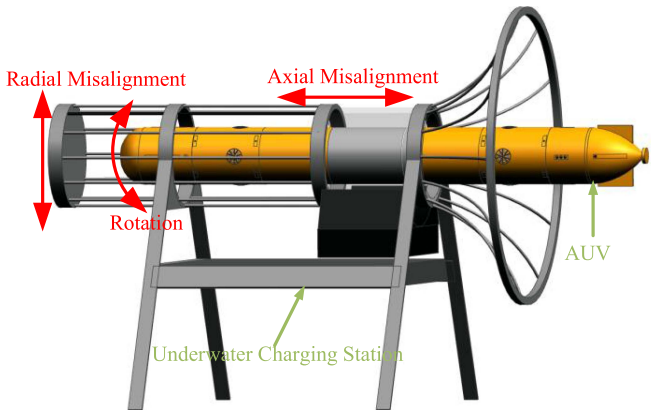


Fig. 1. Sketch of wireless charging station for AUV with misalignment conditions.

Received 16 November 2024; revised 30 January 2025; accepted 22 February 2025. Date of publication 25 February 2025; date of current version 14 April 2025. This work was supported in part by the National Natural Science Foundation of China under Grant 52171338, Grant 52201405, Grant U24B20115, and Grant 52301403, and in part by the Fundamental Research Funds for the Central Universities. Recommended for publication by Associate Editor Y. Tang. *(Corresponding author: Zhengchao Yan.)*

Jiayuan Li, Kehan Zhang, Zhengchao Yan, Baidong Peng, and Jipan Wang are with the School of Marine Science and Technology, Northwestern Polytechnical University, Xi'an 710072, China (e-mail: lijiayuan1998@mail.nwpu.edu.cn; zhangkehan@nwpu.edu.cn; yanzhengchao@nwpu.edu.cn; pbdong@mail.nwpu.edu.cn; jipanwang@mail.nwpu.edu.cn).

Haibing Wen is with the School of Electrical Engineering, Xi'an University of Technology, Xi'an 710048, China (e-mail: wenhaibing@xaut.edu.cn).

Color versions of one or more figures in this article are available at https://doi.org/10.1109/TPEL.2025.3545653.

Digital Object Identifier 10.1109/TPEL.2025.3545653

is alleviating variation of $k$ during the coil malposition. Yan et al. [2] proposed a novel magnetic coupler for the AUV with two decoupled transmitter coils and a segmented arc solenoid receiver coil, which significantly ameliorate the fluctuation of $k$ under the rotational and axial misalignment of the receiver coil. A $U$-shaped bipolar transmitter coil and an arc-shaped unipolar receiver coil was presented in [9] for achieving wide-range of the rotation misalignment tolerance. Experiment results showed that the power transfer efficiency of the proposed WPT system are all over 88% within a rotation angle of 240°. In order to enhance misalignment tolerance in radial direction, Zeng et al. [10] optimized a hybrid transmitter structure composed of conical and planar spiral coils. The mentioned construction could generate uniform magnetic area and guarantee stable power "pick up" by the receiver side. By the way, the receiver coil with circular architecture enables the anti-rotational misalignment tolerance in above WPT system. Besides, a magnetic coupler with uniform horizontal magnetic flux was established to improve the rotational and axial misalignment tolerance [11], which was utilized a quadruple-coil transmitter coil and a crossed dipole receiver coil. The above magnetic coupler also has the preponderance of being lightweight and compact. A portable omnidirectional magnetic resonant extender was designed as an intermediate device to enhance the stability of the underwater WPT system under long distance [12]. Nevertheless, the current research has not further considered achieving constant current output when both the load resistance and coupling coefficient vary.

On the other hand, the research about compensation and control topology of WPT system for AUV is also another method for improving misalignment tolerance. The dc–dc converter attached to receiver side could effectively ensure the stability of the system's output power [13]. Besides, in [14], an S-S compensation topology with variable inductor on receiver side was proposed for AUV WPT system, which could maintain constant current output with wide variation of coupling coefficient. Lin et al. [15] proposed a *LCC*-SS topology with an innovatively magnetic coupler and two rectifiers for coping with rotational and axial misalignment. A fly in the ointment, the additional components would still increase volume and weight of the receiver side, which do not meet the compact and lightweight requirements of the AUV. Some topologies with fewer devices on the receiver side have certain adaptability towards above mentioned demands, such as *LCC*-N [16], [17], *LCC*-P [18], and *LCL*-N [19]. In [17] a primary-side linear control method was proposed for constant current/voltage charging for WPT system. However, the mentioned WPT system was lack of misalignment tolerance. Besides, Zhang et al. [16] proposed a constant current/voltage charging method based on *LCC*-N WPT system with frequency modulation, which rely on the high-speed communication between transmitter side and receiver side, thus it is not suitable for underwater environments due to the severe attenuation caused by seawater to high-frequency signals. Hence, some controlled method based on real-time communication, such as frequency modulation control [20], phase shifted control [21] and additional dc–dc converter on transmitter side [22], are not inappropriate for AUV WPT system.

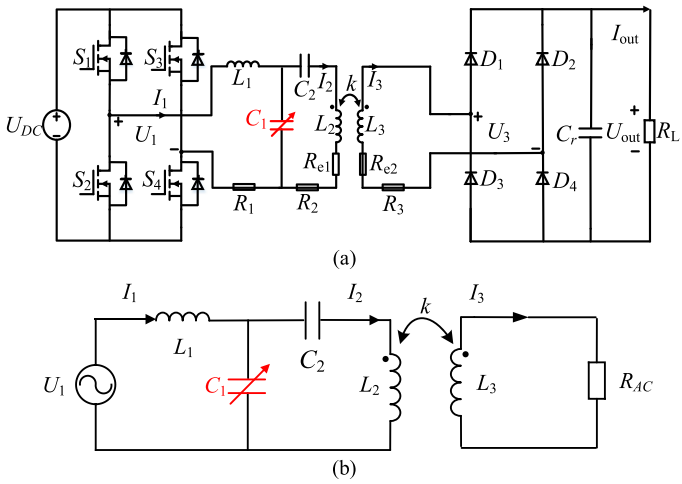


Fig. 2. (a) Proposed AUV WPT system with LCC-N topology. (b) Simplified equivalent AC circuit of proposed WPT system.

Regarding the above issues, this article presented a compact underwater non-communication WPT system with load-independent current output characteristic under wide range of coupling coefficient. The main contribution of this article focuses on the following points.

1) The input-output characteristic of *LCC*-N WPT system is discussed in detail. A control method based on frequency modulation and SCC technology in the transmitter side is designed for the mentioned WPT system, which maintains stable output current when the load resistance and coupling coefficient change.
2) Combining the proposed WPT system, this article also presents an approach to estimate the coupling coefficient based on the primary electrical parameters, which could avoid communication modules between the power transmitter and receiver side.
3) According to experimental results, the proposed WPT system could stable output current while $k$ varies from 0.3 to 0.54 and power transfer efficiency could be maintained above 87%. Besides, the feature of compact receiver side is beneficial for improving the performance of AUV wireless charging.

## II. Theoretical Analysis

Fig. 2(a) shows the proposed WPT system with LCC-N compensation topology for the AUV wireless charging. $S_1 \sim S_4$ are four MOSFETs and $D_1 \sim D_4$ are four diodes. $L_2$ and $L_3$ are the self-inductances of the transmitter coil and receiver coil, respectively. $k$ represents the coupling coefficient between $L_2$ and $L_3$. $C_1$ and $C_2$ are the compensation capacitors on the transmitter side and form an *LCC* topology with the compensation inductance $L_1$. It is worth noting that $C_1$ is constituted with switch-controlled capacitance (SCC). Besides, $C_{\rm r}$ is the filter capacitor on the rectifier. $R_L$ is the load resistance and $R_1$, $R_2$, $R_3$ are the parasitic resistances of corresponding inductors. $R_{e1}$ and $R_{e2}$ represent the eddy current resistances generated by the underwater environment.

Fig. 2(b) presents the equivalent ac circuit of Fig. 2(a), while the resistance of coils and eddy current resistance are ignored for reducing the complexity of system design. It is worth mentioning the reason why eddy current losses could be ignored is that the operating frequency of the system is less than 200 kHz [2]. According to fundamental approximation method, the ac input voltage $\boldsymbol{U}_1$ and equivalent ac load $R_{\mathrm{AC}}$ could be calculated as following [18]:

$$\boldsymbol{U}_1 = \frac{\pi}{4} U_{\mathrm{DC}} \sin(\omega t) = U_1 \sin(\omega t) \tag{1}$$

$$R_{\mathrm{AC}} = \frac{8}{\pi^2} R_L. \tag{2}$$

Then, combing with Kirchhoff's Voltage Law, the circuit current equation of Fig. 2(b) can be expressed as

$$\begin{bmatrix} \boldsymbol{U}_1 \\ 0 \\ 0 \end{bmatrix} = \begin{bmatrix} X_1 + R_1 & X_{C1} & 0 \\ X_{C1} & X_2 + R_2 & X_M \\ 0 & X_M & X_3 + R_3 + R_{\mathrm{AC}} \end{bmatrix} \begin{bmatrix} \boldsymbol{I}_1 \\ \boldsymbol{I}_2 \\ \boldsymbol{I}_3 \end{bmatrix} \tag{3}$$

where $X_{\mathrm{i}}$ $(i = 1, 2, 3 \ldots)$ are presented as following:

$$\begin{cases} X_M = j\omega k\sqrt{L_2 L_3} \\ X_1 = j\omega L_1 + 1/(j\omega C_1) \\ X_2 = j\omega L_2 + 1/(j\omega C_1) + 1/(j\omega C_2) \\ X_3 = j\omega L_3 \\ X_{C1} = 1/(j\omega C_1) \end{cases} \tag{4}$$

where $\omega$ is the system operating angular frequency. By simplifying (3), the current flowing through each inductance while the parasitic resistance is ignored could be expressed as following:

$$\begin{cases} \boldsymbol{I}_1 = \frac{\left(X_M^2 - R_{\mathrm{AC}} X_2 - X_2 X_3\right)\boldsymbol{U}_1}{R_{\mathrm{AC}} X_{C1}^2 + X_3 X_{C1}^2 + X_1 X_M^2 - R_{\mathrm{AC}} X_1 X_2 - X_1 X_2 X_3} \\ \boldsymbol{I}_2 = \frac{(R_{\mathrm{AC}} + X_3) X_{C1} \boldsymbol{U}_1}{R_{\mathrm{AC}} X_{C1}^2 + X_3 X_{C1}^2 + X_1 X_M^2 - R_{\mathrm{AC}} X_1 X_2 - X_1 X_2 X_3} \\ \boldsymbol{I}_3 = \frac{-X_M X_{C1} \boldsymbol{U}_1}{R_{\mathrm{AC}} X_{C1}^2 + X_3 X_{C1}^2 + X_1 X_M^2 - R_{\mathrm{AC}} X_1 X_2 - X_1 X_2 X_3} \end{cases}. \tag{5}$$

### A. Analysis of Constant Current Output Independent With Load Resistance

According to (5), the output current gain of LCC-N topology could be further simplified as

$$G_{\mathrm{IU}} = \frac{I_3}{U_1} = \frac{1}{\frac{X_1 X_2 - X_{C1}^2}{X_M X_{C1}} R_{\mathrm{AC}} + \frac{X_1 X_2 X_3 - X_3 X_{C1}^2 - X_1 X_M^2}{X_M X_{C1}}}. \tag{6}$$

For the output current independent with load resistance, condition (7) should be satisfied

$$X_1 X_2 - X_{C1}^2 = 0. \tag{7}$$

Under this condition, input resistance $\mathrm{Z_{IN}}$ and input resistance angle $\theta$ could be further calculated as

$$\begin{cases} Z_{\mathrm{IN}} = \frac{X_1 X_M^2}{X_M^2 - R_{\mathrm{AC}} X_2 - X_2 X_3} \\ \theta = \arctan\left(\frac{\mathrm{imag}(Z_{\mathrm{IN}})}{\mathrm{real}(Z_{\mathrm{IN}})}\right) \end{cases} \tag{8}$$

Combined with (8), in order to realize zero phase angle (ZPA) operation for the WPT system, the following condition should be established

$$X_2 X_3 - X_M^2 = 0. \tag{9}$$

Then, $G_{\mathrm{IU}}$ could be further expressed as

$$G_{\mathrm{IU}} = \frac{1}{\omega^2 k \sqrt{L_2 L_3} C_1 (\omega L_1 - \frac{1}{\omega C_1})}. \tag{10}$$

While (7) and (9) are satisfied, the output current independent of $R_{\mathrm{AC}}$ with ZPA characteristic could be achieved in LCC-N WPT system. By submitting (4) into (7) and (9), the following solutions could be obtained:

$$\begin{aligned} &\text{Solution 1}: \begin{cases} \omega = \sqrt{\frac{k(L_2(L_2k^2-4L_1))^{\frac{1}{2}} - 2L_2 + L_2k^2}{2\left(C_2L_2^2k^2 - C_2L_2^2 + C_2L_1L_2k^2\right)}} \\ C_1 = \frac{1}{\omega^2(1-k^2)L_2 - \frac{1}{C_2}} \end{cases} \\ &\text{Solution 2}: \begin{cases} \omega = \sqrt{\frac{k(L_2(L_2k^2+4L_1))^{\frac{1}{2}} - 2L_2 + L_2k^2}{2\left(C_2L_2^2k^2 - C_2L_2^2 + C_2L_1L_2k^2\right)}} \\ C_1 = \frac{1}{\omega^2(1-k^2)L_2 - \frac{1}{C_2}} \end{cases} \end{aligned}. \tag{11}$$

Equation (11) shows the values of $\omega$ and $C_1$ which are satisfied for output current independent with $R_{\mathrm{AC}}$ and maintained ZPA operation in the LCC-N WPT system. Fig. 3 shows the input impedance angle and current gain vary with the system frequency under different coupling coefficients to prove correlation properties.

As can be seen from Fig. 3(a), under different load resistance, input impedance angle and output current gain change trend with frequency are distinct. However, there are two frequency point corresponded to solution 1 and solution 2 that the current gain is almost constant at different load resistance condition. Meanwhile, it could be observed that the input impedance angle of the system is zero at these two frequencies, which means that the ZPA characteristic could also be verified. In addition, comparing Fig. 3(a) with and Fig. 3(b), the variation of coupling coefficient would not affect above characteristic.

Hence, for the *LCC*-N WPT system, while *k* changes due to the coil misalignment, it could be guaranteed that the system output current is independent of the load resistance and the ZPA operation can be maintained by adjusting the system operating frequency and compensating the capacitance $C_1$. It is worth noting that to reduce the impact of eddy current loss on system, Solution 1 with lower frequency is selected as system operating frequency. Besides, by contrasting the $G_{\mathrm{IU}}$ under different coupling coefficients in Fig. 3(a) and (b), it can be found that *k* has little effect on the value of system output current, more detailed analysis about the misalignment tolerance of the proposed WPT system is conducted in the following chapter.

### B. Misalignment Tolerance Analysis and Compensation Parameter Design of Proposed WPT System

From (10), there are many fixed parameters that will affect the value of the output current gain when *k* changes, which include $L_1$, $L_2$, $C_2$ and $L_3$. Among them, $L_2$ and $L_3$ are determined by the magnetic coupler. Thereby, discussion focuses on the influence law of $L_1$ and $C_2$ on $G_{IU}$ when *k* changes. Fig. 4 shows the normalized $G_{\mathrm{IU}}$ varies with *k* in different $L_1$.

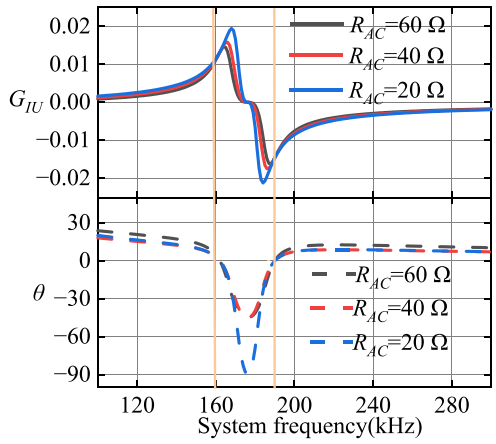


(a)

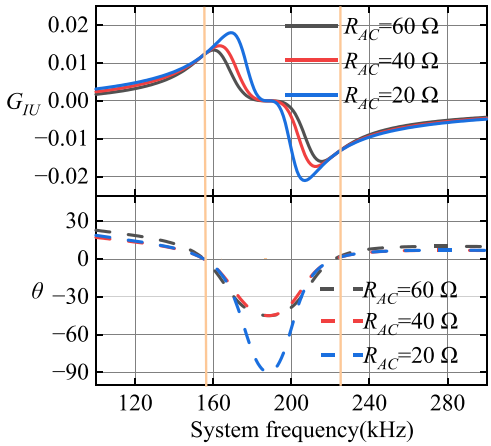


(b)

Fig. 3. (a) Load-independent current gain with ZPA operation at $k = 0.3$. (b) Load-independent current gain with ZPA operation at $k = 0.54$.

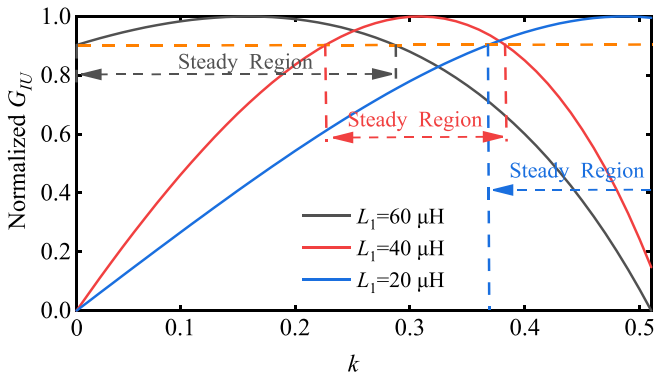


Fig. 4. Normalized $G_{\mathrm{IU}}$ varies with $k$ in different $L_1$.

By observing the orange dashed line in Fig. 4 (the output current in region where normalized $G_{\mathrm{IU}}$ is greater than 0.9 is considered as stable [5]), there is a region where the output current could be maintained stable with certain range of $k$ variation, which is decided by $L_1$. For example, while $L_1 = 60\,\mu$H, $G_{\mathrm{IU}}$ could be considered stable when $k$ varies from 0.01 to 0.29, as shown the black dashed line in Fig. 4. If the steady region is inclined to 0.22 to 0.38, $L_1 = 40\,\mu$H should be satisfied, as shown the red dashed line in Fig. 4. Therefore, it can be ensured the stability of the output current by adjusting the value of compensation parameter $L_1$

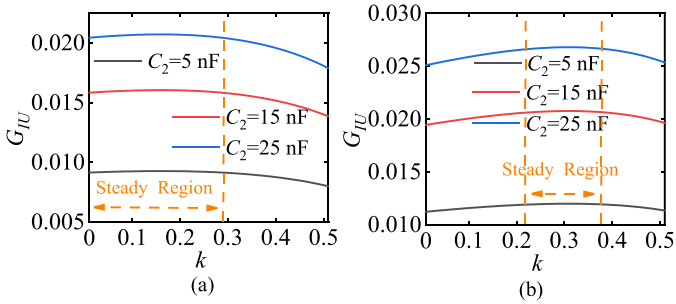


(a) (b)

Fig. 5. Influence law of $C_2$ on $G_{\mathrm{IU}}$. (a) $L_1 = 60\,\mu$H. (b) $L_1 = 40\,\mu$H.

Conversely with $L_1$, as shown in Fig. 5(a) and (b), the fluctuations range of $G_{\mathrm{IU}}$ caused by $k$ variation is not related with $C_2$, which only decided the effective value of the output current. It should be noted that the steady region in Fig. 5 is defined based on a normalized $G_{\mathrm{IU}}$ greater than 0.9. Therefore, the misalignment tolerance of the proposed WPT system could be improved by adjusting $L_1$. In order to ensure a sufficiently large stable as much as possible, the condition of $k = k_{\max}$ should be satisfied at the boundary of steady region (where $k_{\max}$ presents max coupling coefficient between coils in the case of relative position changes). For achieving this, the following conditions need to be met:

$$G_{\mathrm{IU}}|_{k=k_{\max}} = 0.9 \times \mathrm{Max}\,(G_{\mathrm{IU}}) \tag{12}$$

where $\mathrm{Max}(G_{\mathrm{IU}})$ is the maximum value of $G_{\mathrm{IU}}$ when $k$ varies from 0 to 1, which could be calculated by deriving $G_{\mathrm{IU}}$ to $k$ as shown in the following equation:

$$\frac{\partial G_{\mathrm{IU}}}{\partial k} = 0. \tag{13}$$

It could be obtained $k = k_0$ which is the solution of (13). Due to the complex algebraic relationships in above equation, the solving process could be carried out through numerical calculation software MATLAB.

Although the value of $C_2$ would not affect the variation tendency of $G_{IU}$ when $k$ change, it will determine the variation range of $C_1$ and $\omega$ when $k$ changes, as shown in Fig. 6.

As can be seen from Fig. 6, while $C_2 = 5\,$nF, the change in $k$ requires the system operating frequency to be maintained above 200 kHz. Under this frequency range, the eddy current loss of the underwater WPT system will cause a significant impact on the input and output characteristic of the system, which is not conducive to its efficient operation. Reasonably adjusting the value of $C_2$ could diminish the range of system operating frequency changes, thereby reducing the system losses. To sum up, the parameter design process of the proposed WPT system is shown in Fig. 7.

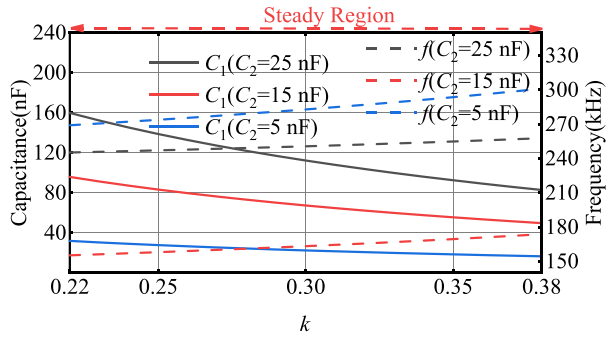


Fig. 6. Variation scope of $C_1$ and $\omega$ when the coupling coefficient change in steady region.

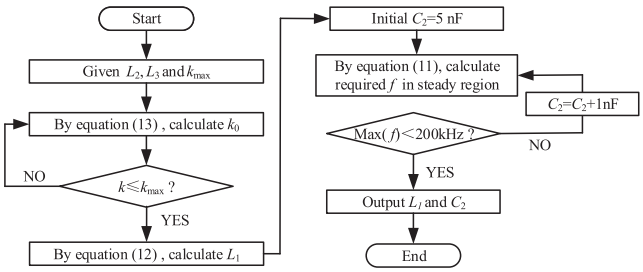


Fig. 7. Flowchart of compensation parameter design.

### C. Coupling Coefficient Estimation

According to the above analysis, in the operating process of the proposed WPT system, the value of $C_1$ and $\omega$ are determined by $k$. Hence, an approach is needed to estimate the coupling coefficient between coils. However, due to the instability of communication in marine environment, it prefers to estimate the coupling coefficient through electrical parameters on the transmitter side.

The proposed WPT system is starting operating after configuring $C_1$ and $\omega$ through $k_{\max}$. While the misalignment occurs between the AUV and underwater power supply station, $k < k_{\max}$, the established working state would be disrupted. More detailed, under established system parameters, the variation of $k$ would break condition (9), which would not affect condition (7). This will cause a phase difference between the system output current and voltage. Furthermore, there is an imaginary part in the system input impedance when $k < k_{\max}$, and could be expressed as following:

$$\text{imag}(Z_{\text{in}}) = \left| \frac{a^2 X_1 X_M^2}{a^2 X_M^2 - X_2 X_3} \right| = \frac{a^2}{a^2 - 1} \left( \omega L_1 - \frac{1}{\omega C_1} \right) \tag{14}$$

where $a$ denotes the misalignment degree of receiver coil and $k = ak_{\max}$. Thereby, the coupling coefficient could be estimated by detecting the input current, input voltage and phase between them (imaginary part of input impedance). Then, the coupling coefficient can be obtained according to the following equation:

$$\begin{cases} k = k_{\max} \sqrt{\dfrac{\text{imag}(Z_{\text{in}})}{\text{imag}(Z_{\text{in}}) - \omega L_1 + \frac{1}{\omega C_1}}} \\ \text{imag}(Z_{\text{in}}) = \left| \dfrac{U_1}{I_1} \right| \sin\theta \end{cases}. \tag{15}$$

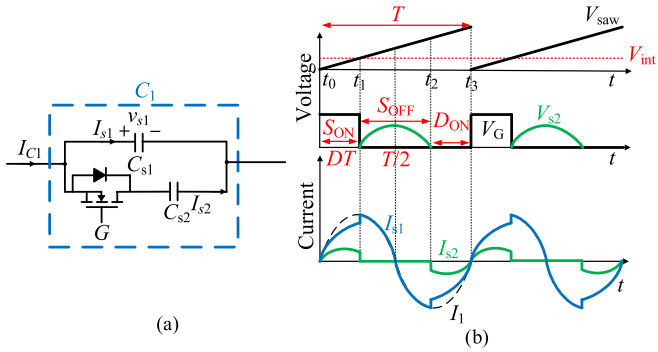


Fig. 8. Configuration of SCC. (a) Structure of SCC. (b) Key waveforms of SCC.

## III. Control Strategy for Proposed WPT System

### A. Configuration of Switched-Controlled Capacitance

The continuous adjusting of $C_1$ with the variation of $k$ is achieved through switched-controlled capacitance technology. The circuit diagram of SCC is shown in Fig. 8(a), among them, a controlled MOSFET in series with $C_{s2}$ and then in parallel with $C_{s1}$. Capacitor $C_{s2}$ is connected in series to reduce the voltage stress on the switch. The key waveforms of SCC are shown in Fig. 8(b). Comparing the modulation signal $V_{\text{int}}$ with the sawtooth wave to generate the gate driving signal $V_G$ and recording the duty cycle as $D$ which directly determining the value of equivalent capacitance of SCC. It is worth noting that the rising edge of $V_G$ always aligns with the positive zero crossing point of the total current flowing through SCC. In addition, when $D$>0.5, the branch of $C_{s2}$ always maintains continuity, hence the effective range of $D$ is [0, 0.5].

Regarding the calculation of SCC, the analytical solution of duty cycle can be directly obtained through the charge ratio method, which is more accurate than the duty cycle obtained by the fundamental wave approximation method. The equivalent capacity value $C_1$ of SCC can be regarded as the sum of the capacity values of the upper and lower branches. The capacity value of the upper branch is $C_{s1}$, while the equivalent capacity value of the lower branch depends on the switch state and can be recorded as $C_{S2\text{eq}}$, then the following equation could be obtained:

$$C_1 = C_{s1} + C_{s2\text{eq}}. \tag{16}$$

According to the formula $C = \Delta Q/\Delta U$, the capacitance values of both the upper and lower branches can be expressed as the ratio of their respective charge increments and voltage changes over a certain period of time. Due to the parallel connection between the two branches, $\Delta U$ is always equal during any time period, therefore it can be concluded that

$$\frac{C_{s2\text{eq}}}{C_{s1}} = \frac{\Delta Q_{s2}}{\Delta Q_{s1}} \Rightarrow C_{s2\text{eq}} = \frac{\Delta Q_{s2}}{\Delta Q_{s1}} C_{s1}. \tag{17}$$

Assuming the expression for the total current $I_{c1}$ is $I_{c1}(t) = I_m \sin(\omega t)$, according to diversion relationship, the two branch

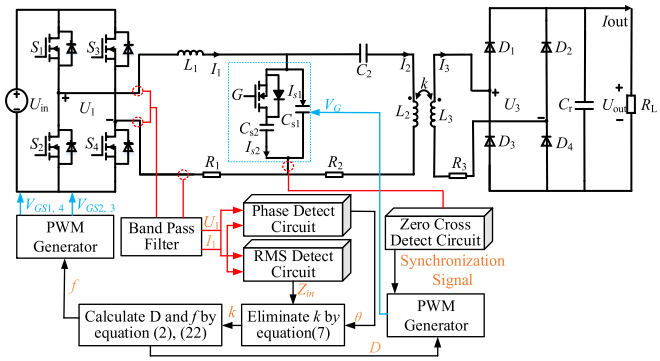


Fig. 9. Control diagram for proposed WPT system.

currents can be expressed as

$$I_{cs1}(t) = \begin{cases} \frac{C_{s1}}{C_{s1}+C_{s2}} I_m \sin(\omega t), t = (0, DT) \cup ((1-D)T, T) \\ I_m \sin(\omega t), t = (DT, (1-D)T) \end{cases}$$

$$I_{cs2}(t) = \begin{cases} \frac{C_{s2}}{C_{s1}+C_{s2}} I_m \sin(\omega t), t = (0, DT) \cup ((1-D)T, T) \\ I_m \sin(\omega t), t = (DT, (1-D)T) \end{cases}. \quad (18)$$

Then integrating $I_{cs1}(t)$ and $I_{cs2}(t)$ within $t = [0, 0.5T]$, the charge on each capacitor could be indicated as

$$\Delta Q_{s1} = \int_0^{0.5T} I_{cs1}(t)dt = \frac{C_{s1}}{C_{s1}+C_{s2}} I_m(1-\cos 2D\pi) + I_m(1+\cos 2D\pi) \quad (19)$$

$$\Delta Q_{s2} = \int_0^{0.5T} I_{cs2}(t)dt = \frac{C_{s2}}{C_{s1}+C_{s2}} I_m(1-\cos 2D\pi). \quad (20)$$

By combining (15) to (19), $C_1$ can be explicit expression for duty cycle $D$ as

$$C_1 = \frac{2C_{s1}(C_{s1}+C_{s2})}{2C_{s1}+(1+\cos 2D\pi)C_{s2}}, C_1 \in [C_{s1}, C_{s1}+C_{s2}]$$
$$\Rightarrow D = \frac{1}{2\pi} \arccos \frac{2C_{s1}(C_{s1}-C_1)+C_{s2}(2C_{s1}-C_1)}{C_1 C_{s2}}. \quad (21)$$

### B. Control Strategy for Proposed WPT System

According to the SCC technology, the control diagram for the proposed WPT system is presented in Fig. 9. $U_1$ and $I_1$ collected by voltage and current sensors are sent to the phase and RMS detection circuit, simultaneously. Band pass filters are used for improving measurement accuracy. DSP is employed to process the signal output from phase and RMS detection circuit and estimate the coupling coefficient through it. Meanwhile, in DSP, it is also need to calculate $D$ and $f$ according to (2), (11), and (21), and output corresponding PWM signals.

The working principle of the mentioned phase detection circuit, RMS detection circuit and zero cross detection circuit are as follows: for phase detection circuit, which is composed with two compere and a JK flip-flop, the square wave signal output by it is sent to the enhanced capture (ECAP) module of DSP to calculate the duty cycle and obtain $\theta$; the voltage signal output by RMS detection circuit is sent to general purpose input/output (GPIO) of digital signal processor (DSP) to obtain $Z_{in}$; the square wave output by the zero crossing detection circuit with compere is sent to the DSP ECAP module to capture its rising edge time and generate the synchronization signal of SCC.

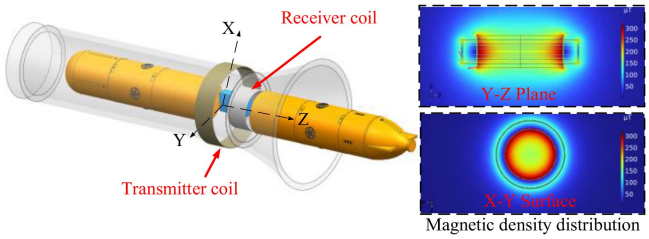


Fig. 10. Magnetic coupler structure and magnetic field distribution for proposed AUV wireless power transfer system.

TABLE I
MAGNETIC COUPLER PARAMETERS

| *Parameters* | *Simulation* | *Measurement* |
|---|---|---|
| Self-inductance $L_2$ | 85 $\mu$H | 86.842 $\mu$H |
| Self-inductance $L_3$ | 85 $\mu$H | 88.609 $\mu$H |
| Diameter of transmitter coil $d_1$ | 270 mm | 270 mm |
| Diameter of receiver coil $d_2$ | 200 mm | 200 mm |
| Turn of transmitter coil $N_1$ | 14 | 14 |
| Turn of receiver coil $N_2$ | 19 | 19 |

### C. Magnetic Coupler for AUV WPT System

To verify the feasibility and misalignment tolerance of proposed LCC-N WPT system for the AUV, a spiral coil with simple structure and its easy-winding characteristic are adopted as a magnetic coupler. The magnetic coupler structure and magnetic field density of proposed WPT system for the AUV is presented in Fig. 10 with the assistance of multi-physics simulation software COMSOL.

For relieving the skin effect, Litz wires (400 strands with a diameter of 3.9 mm) are adopted to wind the mentioned magnetic coupler. The related simulation and measured parameters of the magnetic coupler are given in Table I.

Fig. 11(a), (b), and (c) shows the simulation and measurement results of the coupling coefficients vary with different misalignment conditions of receiver coil.

As shown in Fig. 11(a), the coil has not experienced radial misalignment, while the axial misalignment distance of the receiver coil varies from 0 to 80 mm, the coupling coefficient changes from 0.54 to 0.3. At the same time, Fig. 11(a) also shows the variation of coupling coefficient with only rotational misalignment in the receiver coil. The results show that the

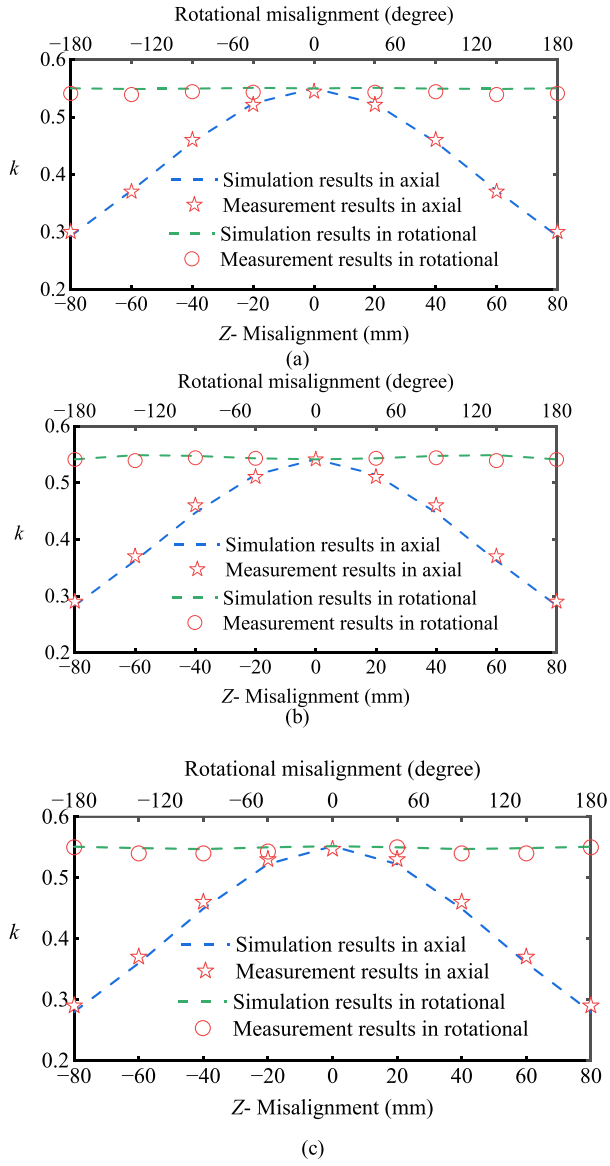


Fig. 11. Variation of coupling coefficient with different misalignment. (a) $y = 0$ mm. (b) $y = \pm 10$ mm. (c) $y = \pm 20$ mm.

proposed magnetic coupler has a satisfactory performance in antirotational misalignment.

Besides, by comparing Fig. 11(a), (b), and (c), while the axial misalignment degree varies from 0mm to 80mm, the coupling coefficients decrease from 0.54 to 0.3, 0.544 to 0.3 and 0.55 to 0.29 in $y = 0$ mm, $y = 10$ mm, and $y = 20$ mm, respectively. It can be concluded that there is a minor change in coupling coefficient when radial misalignment occurs. The mentioned results also indicate that the simulated value are agree well with the measured values.

In order to reduce the complexity of the experiment, the input-output characteristics of the experimental prototype were only validated with an axial misalignment from $-80$ mm to 80 mm ($y = 0$ mm). One reason for this is that the coupling coefficient of the magnetic coupler structure changes relatively little when the receiving coil undergoes radial and axial displacement. On

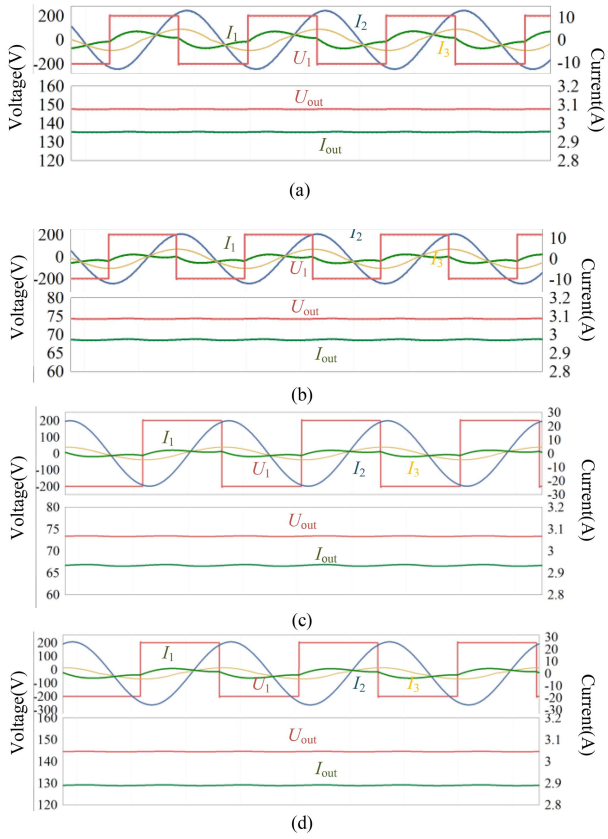


Fig. 12. Simulation results of input and output characteristic. (a) $R = 25\ \Omega$ and $k = 0.4$. (b) $R = 50\ \Omega$ and $k = 0.4$. (c) $R = 25\ \Omega$ and $k = 0.2$. (d) $R = 50\ \Omega$ and $k = 0.2$.

the other hand, this article mainly studies the misalignment tolerance of the proposed *LCC*-N WPT system for AUV when the coupling coefficient varies, without paying attention to how the coupling coefficient changes.

## IV. Simulation Analysis and Experimental Verification

### A. Simulation Analysis

To verify the misalignment tolerance of the proposed WPT system, relevant models were built in PSIM simulation software and Fig. 12 shows the simulation results.

As can be seen from Fig. 12, the output current of the system is not affected by the coupling coefficient and load resistance. In addition, by observing input current $I_1$ and voltage $U_1$ in Fig. 12(a), (b), (c), and (d), ZPA characteristic could be maintained during the system operation. Detailed analysis and verification would be presented combined with experiment results as presented in following.

### B. Experimental Validation

To prove the feasibility and superiority of the above theoretical analysis, an experimental prototype with 2 A output current is established, as shown in Fig. 13. The four MOSFETs compose with inverter are GS66508B and the four diodes used on rectifier are

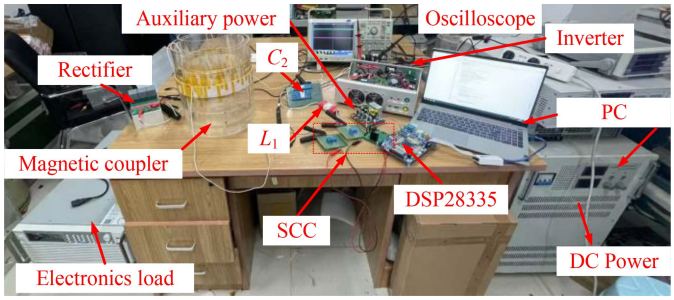


Fig. 13. Experimental platform of *LCC*-N WPT system for AUV.

TABLE II
SYSTEM PARAMETERS

| *Parameters* | *Value* | *Parameters* | *Value* |
|---|---|---|---|
| $L_1$ | 41 $\mu$H | $C_{s1}$ | 25 nF |
| $C_2$ | 15 nF | $C_{s2}$ | 65 nF |
| $f$ | 153–193 kHz | $C_1$ | 29.8–77.3 nF |
| $U_1$ | 140 V | $R_L$ | 25–200Ω |

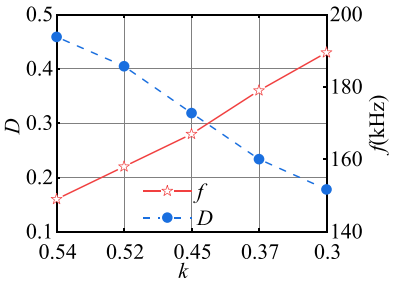


Fig. 14. Duty cycle of SCC and system operating frequency was adopted with different coupling coefficient during the experiment.

IV1D12030U3. The MOSFET adopted by SCC is C2M0080120D with a withstand voltage of 1200 V. The driving signals for the inverter and SCC are generated by DSP28335. The variation of the load resistance is achieved by the electronic load. At the same time, to simulate the operation of the WPT system in seawater environment, the gap between the transmitter coil and receiver coil is filled up saltwater with a salinity of 4‰. In addition, according to Fig. 7 and combing the variation of $k$ by the magnetic coupler in Fig. 11, the compensation parameters and system operating frequency could be calculated and given in Table II.

Fig. 14 shows the duty cycle of SCC and system operating frequency under different $k$ adopted in the experiment. To verify the misalignment tolerance of the proposed WPT system, the output current of the system was measured while misalignment in $Z$-direction is 0, 20, 40, 60, and 80 mm, and the corresponding coupling coefficient is $k = 0.54$, $k = 0.52$, $k = 0.45$, $k = 0.37$, and $k = 0.3$, respectively, the results are shown in Fig. 15.

As can be seen from Fig. 14, for the proposed WPT system, the output current of system could remain stable around 2A when the receiver coil is malposition, and the change in load resistance will not affect this characteristic. Specifically, while receiver coil is not misaligned ($k = 0.54$), corresponds to $D = 0.16$ and $f = 193$ kHz ($C_1 = 30.2$ nF), the output current is

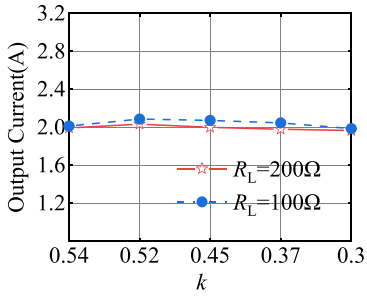


Fig. 15. Output current of proposed WPT system with magnetic coupler misalignment.

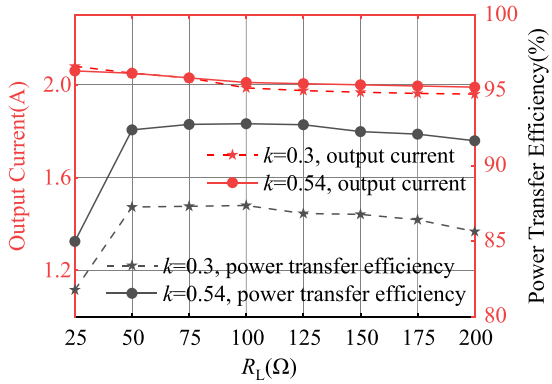


Fig. 16. Power transfer performance of proposed WPT system under seawater environment.

1.99 A and 2.01 A at $R_L = 200\,\Omega$ and $100\,\Omega$, respectively. When the receiver coil experiences a 20mm axial misalignment, the coupling coefficient is 0.52. At this time, the system operates at $D = 0.22$ and $f = 185$ kHz ($C_1 = 34.3$ nF), with output currents of 2.08 A and 2.03 A at $R_L = 100\,\Omega$ and 200 Ω, respectively. While $k = 0.45$ corresponds to $D = 0.28$ and $f = 172$ kHz ($C_1 = 43.5$ nF), the output current is 2.05 A and 2.07 A at $R_L = 200\,\Omega$ and 100 Ω, respectively. For 60 mm misalignment of receiver coil, $k = 0.36$ with $D = 0.36$ and $f = 160$ kHz, output current is 1.98 A and 2.04 A at $R_L = 200\,\Omega$ and 100 Ω, respectively. At maximum misalignment ($z = 80$ mm, $k = 0.3$), $D$ and $f$ are set as 0.43 and 153 kHz, respectively. Under this state, the output current could also be maintained in 1.96A and 1.98A when the load resistance is 200 and 100 Ω.

Based on the above results, it can be concluded that the fluctuation of the system output current is 4.47% when the coupling coefficient varies from 0.54 to 0.3, which could effectively meet the misalignment requirement of the AUV WPT system. On the other hand, the main reason for the fluctuation of output current is the inaccurate estimation of the coupling coefficient. This article is based on the absence of communication between the AUV and charging stations. If a reliable communication between the primary and secondary sides is built, the system working status can be further accurately determined based on the output current for achieving higher precision system output characteristic when the misalignments occur.

Fig. 16 shows the power transfer efficiency performance of the proposed WPT system under seawater environment.

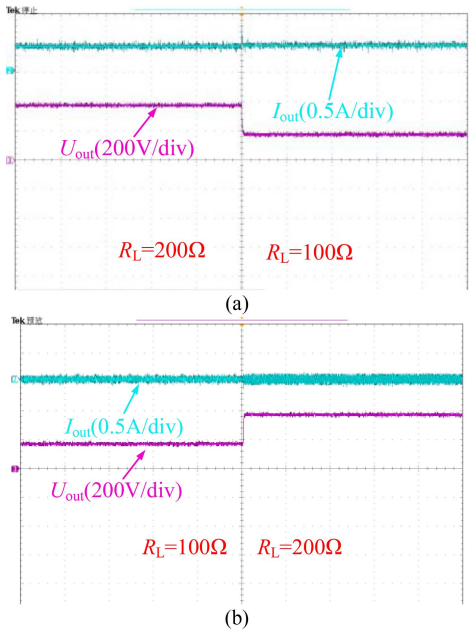


Fig. 17. Waveform of output voltage and current at the moment of load resistance switching. (a) $k = 0.53$. (b) $k = 0.3$.

For the proposed *LCC*-N WPT system, while $R_L$ varies from 25 to 200 Ω, the output current could be sustained in 2 A or so, which basically achieved constant current output independent of the load resistance. To be more specific, when $k = 0.53$ and $R_L$ changes from 25 to 200 Ω, the output current varies from 2.06 to 1.99 A and the volatility of the output current is 3.3%. In addition, the maximum power transfer efficiency can arrive 92.8% at $R_L = 100\,\Omega$ when the receiver coil is aligned. At the same time, efficiency could also be maintained above 85% when the load resistance changes from 25 to 200 Ω. Besides, while $k = 0.3$, the maximum power transfer efficiency could arrive 87.38% at $R_L = 100\Omega$ and when $R_L$ varies from 25 to 200 Ω, efficiency of 81.78% is able to achieved.

Fig. 17(a) shows the performance in the system output current and output voltage when the load resistance switches from 200 to 100 Ω under $k = 0.53$. When the load resistance switches from 200 to 100 Ω, the output current remains almost unchanged while the system output voltage doubles. Similarly, when $k = 0.3$ and $R_L$ changes from 25 to 200 Ω, the output current varies from 2.08 to 1.96 A, the fluctuation of the output current is 5.7%. Meanwhile, from Fig. 17(b), when $R_L$ switches from 100 to 200 Ω under $k = 0.3$, the output current remains almost unchanged while the system output voltage is halved.

Fig. 18 shows the voltage and current waveforms of the system. The system operating frequency is set to 193 kHz under $k = 0.54$ and by comparing Fig. 18(a) and (b), the phase between the input voltage $U_1$ and $I_1$ is zero while $R_L = 200\,\Omega$ and 100 Ω. Similarly, while $k = 0.3$, the system operating frequency is set to 153 kHz and the change of load resistance would not affect the phase between $U_1$ and $I_1$. Hence, it could be concluded that the ZPA characteristic of system could be maintained while $k$ and $R_L$ change, which is beneficial for the efficient operation of the system.

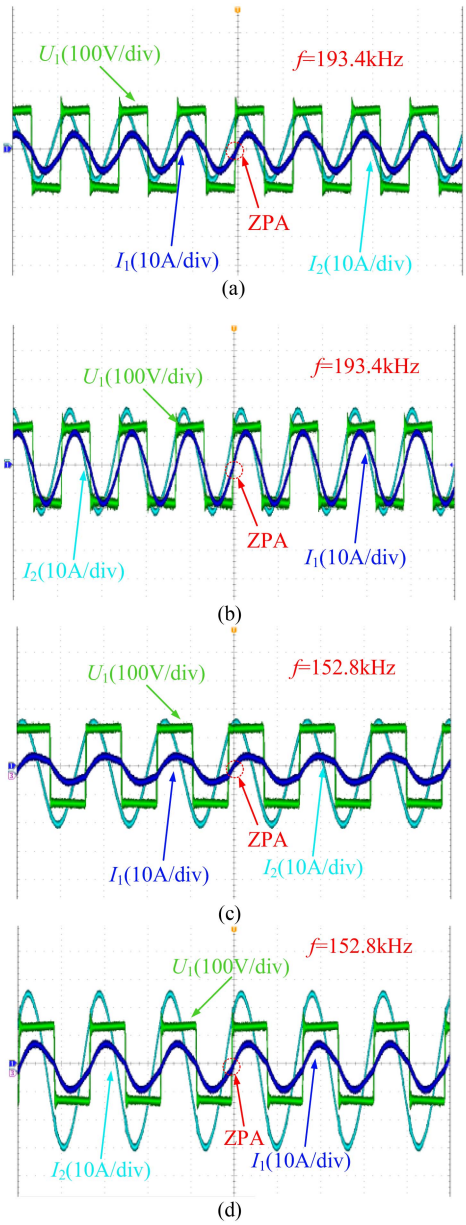


Fig. 18. Related waveform of input characteristic when $k$ and $R_L$ change. (a) $k = 0.54$ and $R_L = 200\,\Omega$. (b) $k = 0.54$ and $R_L = 100\,\Omega$. (c) $k = 0.3$ and $R_L = 200\,\Omega$. (d) $k = 0.3$ and $R_L = 100\,\Omega$.

Table III compares four misalignment tolerance technologies currently applicable to AUV WPT system under non-communication condition, including system output power fluctuation, maximum efficiency, components on receiver side and whether the receiver side is compact and lightweight. As can be seen from Table III, by using detuned topology and variable inductance, the misalignment tolerance could be further improved within a wide range of coupling coefficient variations. However, the integration of a large number of components at the receiver side is not conducive to the compactness and lightweight of the system. On the other hand, the method of magnetic coupling design could reduce the difficulty of system design and control complexity while ensuring the misalignment

TABLE III
COMPARISON STUDY WITH THE RELEVANT WORKS

| References | Hong et al. [23] | Li et al. [14] | Wang et al. [24] | This article |
|---|---|---|---|---|
| Strategy | Detuned topology | Variable inductor | Magnetic coupler design | SCC + Frequency modulation |
| Magnetic coupler | 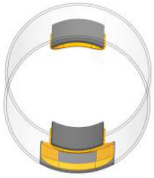 | 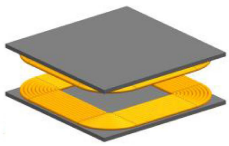 | 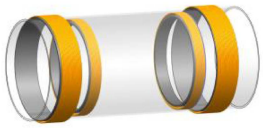 |  |
| $k$ variation with misalignment | Axial: 0.2-0.6 [±100 mm]<br>Rotational: 0.2-0.6 [±30°] | *XY*-: 0.15-0.5[±140 mm]<br>*Z*-: 0.15-0.5[0 ~90 mm] | Axial: 0.065-0.074 [±100 mm]<br>Rotational: 0.074-0.074 [±180°] | Axial: 0.3–0.54 [±80 mm]<br>Rotational:0.54–0.54 [±180°] |
| Power fluctuation with misalignment | 8% | 4.5% | 11.7% | 4.47% |
| Max efficiency | 88% | 96.1% | 93% | 92.8% |
| Components in the receiver side | Two rectifier and two capacitor | Variable inductor and a capacitor and a rectifier | Capacitor and + a rectifier | Rectifier |
| Compact/lightweight on receiver side | NO | NO | NO | YES |
| Communication | NO | NO | NO | NO |

tolerance of WPT system. However, when the magnetic coupler was misaligned, the system output power fluctuates greatly. The WPT system proposed in this article for AUV could achieve lower fluctuations in system output power within a wide range of coupling coefficient variations, while effectively guarantee that the compactness and weight of the receiver side, making it very suitable for WPT systems with high requirements for the volume and weight of the secondary side.

## V. CONCLUSION

This article presented an *LCC*-N WPT system with fewer compensation devices on the receiver side for the AUV. By adjusting the compensation capacitor and system operating frequency, the output current of the WPT system could maintain stable while the coupling coefficient $k$ undergoes a wide range variation. Meanwhile, the output current is independent of the load resistance and ZPA could also be well maintained. Besides, a control method was proposed which does not require communication between the transmitter and receiver side in underwater environment. An underwater WPT system with 2 A output current has been built to prove the relevant theoretical analysis and simulation results. The experimental results indicate that while the coupling coefficient varies from 0.3 to 0.54, the fluctuation of output current is less than 4.47% and the power transfer efficiency could be maintained above 87%, and the maximum efficiency can reach 92.8%. In addition, the load-independent characteristic of the output current could maintain during the misalignment process was also verified.

## REFERENCES

[1] Z. Yan et al., "An underwater wireless power transfer system with improved misalignment tolerance," *IEEE J. Emerg. Sel. Top. Power Electron.*, to be published, doi: 10.1109/JESTPE.2025.3541289.

[2] Z. Yan et al., "Free-rotation wireless power transfer system based on composite anti-misalignment method for AUVs," *IEEE Trans. Power Electron.*, vol. 38, no. 4, pp. 4262–4266, Apr. 2023.

[3] C. R. Teeneti, T. T. Truscott, D. N. Beal, and Z. Pantic, "Review of wireless charging systems for autonomous underwater vehicles," *IEEE J. Ocean. Eng.*, vol. 46, no. 1, pp. 68–87, Jan. 2021.

[4] B. Peng, K. Zhang, Z. Yan, J. Wang, and Z. Mao, "An underwater anti-misalignment UPT system based on array transducers," *IEEE J. Emerg. Sel. Top. Power Electron.*, to be published, doi: 10.1109/JESTPE.2024.3484969.

[5] S. Wu, C. Cai, A. Wang, Z. Qin, and S. Yang, "Design and implementation of a uniform power and stable efficiency wireless charging system for autonomous underwater vehicles," *IEEE Trans. Ind. Electron.*, vol. 70, no. 6, pp. 5674–5684, Jun. 2023.

[6] B. Zhang, J. Chen, X. Wang, W. Xu, C. Lu, and Y. Lu, "High-power-density wireless power transfer system for autonomous underwater vehicle based on a variable ring-shaped magnetic coupler," *IEEE Trans. Transp. Electrific.*, vol. 10, no. 2, pp. 3061–3074, Jun. 2024.

[7] Y. Zhang, H. Zhou, Z. Shen, R. Xie, X. Chen, and X. Mao, "An interoperable dynamic wireless charging system with stable output based on a self-adaptive two-pole receiver," *IEEE Trans. Power Electron.*, vol. 39, no. 10, pp. 11943–11947, Oct. 2024.

[8] Y. Zhang, H. Zhou, Z. Shen, R. Xie, Z. Zheng, and X. Chen, "A family of self-adaptive interoperable receivers based on multiple decoupled receiving poles for electric vehicle wireless charging systems," *IEEE Trans. Power Electron.*, vol. 39, no. 9, pp. 11794–11802, Sep. 2024.

[9] Z. Chen, X. Zhang, F. Xu, M. Li, Z. Yuan, and Q. Yang, "Wide rotation-misalignment-tolerance design of magnetic coupled structure for AUVs wireless charging system," *IEEE Trans. Ind. Electron.*, vol. 71, no. 11, pp. 14086–14096, Nov. 2024.

[10] Y. Zeng et al., "Misalignment insensitive wireless power transfer system using a hybrid transmitter for autonomous underwater vehicles," *IEEE Trans. Ind. Appl.*, vol. 58, no. 1, pp. 1298–1306, Jan./Feb. 2022.

[11] S. Wu, C. Cai, W. Chai, J. Li, Q. Cui, and S. Yang, "Uniform power IPT system with quadruple-coil transmitter and crossed dipole receiver for autonomous underwater vehicles," *IEEE Trans. Ind. Appl.*, vol. 58, no. 1, pp. 1289–1297, Jan./Feb. 2022.

[12] X. Tian, W. Liu, K. T. Chau, and S. M. Goetz, "Omnidirectional magnetic resonant extender design for underwater wireless charging system," *IEEE J. Emerg. Sel. Top. Power Electron.*, vol. 12, no. 4, pp. 3325–3333, Aug. 2024.

[13] D. Wang, J. Zhang, S. Cui, Z. Bie, F. Chen, and C. Zhu, "The state-of-the-arts of underwater wireless power transfer: A comprehensive review and new perspectives," *Renew. Sustain. Energy Rev.*, vol. 189, 2024, Art. no. 113910.

[14] J. Li, C. Zhu, J. Xie, F. Lu, and X. Zhang, "Design and implementation of high-misalignment tolerance WPT system for underwater vehicles based on a variable inductor," *IEEE Trans. Power Electron.*, vol. 38, no. 10, pp. 11726–11737, Oct. 2023.
[15] H. Lin, C. Cai, S. Wu, Y. Jiao, W. Chai, and J. Yu, "Compact and misalignment tolerance IPT system based on sine-cosine coupling superposition for autonomous underwater vehicle applications," *IEEE Trans. Transp. Electrific.*, to be published, doi: 10.1109/TTE.2024.3520319.
[16] Y. Zhang, Z. Shen, H. Wang, W. Pan, and W. Wu, "Analysis and design of constant-current and constant-voltage output for LCC-N topology in wireless power transfer system," in *Proc. IEEE 1st Int. Power Electron. Appl. Symp.*, 2021, pp. 1–5.
[17] Z. Liu, L. Wang, Y. Guo, and S. Li, "Primary-side linear control for constant current/voltage charging of the wireless power transfer system based on the LCC-N compensation topology," *IEEE Trans. Ind. Electron.*, vol. 69, no. 9, pp. 8895–8904, Sep. 2022.
[18] Z. Yan, Y. Zhang, B. Song, K. Zhang, T. Kan, and C. Mi, "An LCC-P compensated wireless power transfer system with a constant current output and reduced receiver size," *Energies*, vol. 12, no. 1, p. 172, 2019, doi: 10.3390/en12010172.
[19] Y. Zhang, Z. Yan, Z. Liang, S. Li, and C. C. Mi, "A high-power wireless charging system using LCL-N topology to achieve a compact and low-cost receiver," *IEEE Trans. Power Electron.*, vol. 35, no. 1, pp. 131–137, Jan. 2020.
[20] Y. Jiang, L. Wang, Y. Wang, J. Liu, M. Wu, and G. Ning, "Analysis, design, and implementation of WPT system for EV's battery charging based on optimal operation frequency range," *IEEE Trans. Power Electron.*, vol. 34, no. 7, pp. 6890–6905, Jul. 2019.
[21] K. Colak, E. Asa, M. Bojarski, D. Czarkowski, and O. C. Onar, "A novel phase-shift control of semi-bridgeless active rectifier for wireless power transfer," *IEEE Trans. Power Electron.*, vol. 30, no. 11, pp. 6288–6297, Nov. 2015.
[22] H. Zhu, B. Zhang, and L. Wu, "Output power stabilization for wireless power transfer system employing primary-side-only control," *IEEE Access*, vol. 8, pp. 63735–63747, 2020.
[23] T. Hong et al., "A self-adaptive dual-channel LCC-S detuned topology for misalignment tolerance in AUV wireless power transfer systems," *IEEE Trans. Power Electron.*, vol. 40, no. 3, pp. 4630–4639, Mar. 2025.
[24] D. Wang et al., "Wide anti-misalignment tolerance WPT system with uniform magnetic field coupler for autonomous underwater vehicles," *IEEE J. Emerg. Sel. Top. Power Electron.*, to be published, doi: 10.1109/JESTPE.2024.3454089.

**Jiayuan Li** was born in Sichuan, China, in 1998. He received the B.S. degree in electrical engineering from the Hunan University of Science and Technology, Xiangtan, China, in 2020, the M.S. degree in electrical engineering from the Xi'an University of Technology, Xi'an, China, in 2024. He is currently working toward the Ph.D. degree in electrical engineering with the Northwestern Polytechnical University, Xi'an, China.

His main research interest includes wireless power transfer.

**Kehan Zhang** (Member, IEEE) received the B.S. and M.S. degrees in control theory and control engineering from Northwestern Polytechnical University, Xi'an, China, in 1993 and 1996, respectively, and the Ph.D. degree in control theory and control engineering from Xi'an Jiaotong University, Xi'an, China, in 2000.

He is currently a Professor with Northwestern Polytechnical University. His research interests focus on DSP-based brushless dc motor control system and wireless power transfer.

**Zhengchao Yan** (Member, IEEE) received the B.S. and Ph.D. degrees in electrical engineering from Northwestern Polytechnical University, Xi'an, China, in 2013 and 2020, respectively.

He was a Joint Ph.D. student with the San Diego State University, San Diego, CA, USA, from 2017 to 2019. From 2020 to 2023, he was an Assistant Professor with Xi'an Jiaotong University, Xi'an, China. He is currently a Professor with Northwestern Polytechnical University. His research interests focus on underwater wireless power transfer.

**Haibing Wen** received the B.S., M.S., and Ph.D. degrees in naval architecture and ocean engineering from Northwestern Polytechnical University, Xi'an, China, in 2010, 2013, and 2021, respectively.

Since 2021, he has been a full-time Postdoctoral Research Fellow with the School of Electrical Engineering, Xi'an University of Technology, Xi'an, China, where he is currently a Lecturer. His research interests include wireless power transfer, including electromagnetic shielding, system optimization.

**Baidong Peng** is currently working toward the doctor's degree in electrical engineering with the School of Marine Science and Technology, Northwestern Polytechnical University, Xi'an, China.

His research interests focus on underwater wireless power transfer.

**Jipan Wang** is currently working toward the master's degree in control science and engineering with the School of Marine Science and Technology, Northwestern Polytechnical University, Xi'an, China.

His research interests focus on underwater wireless power transfer.